AUTHOR QUERY FORM

ELSEVIER	**Journal: PTEC** **Article Number: 8124**	**Please e-mail or fax your responses and any corrections to:** **E-mail: corrections.esil@elsevier.spitech.com** **Fax: +1 619 699 6721**

Dear Author,

Any queries or remarks that have arisen during the processing of your manuscript are listed below and highlighted by flags in the proof. Please check your proof carefully and mark all corrections at the appropriate place in the proof (e.g., by using on-screen annotation in the PDF file) or compile them in a separate list.

For correction or revision of any artwork, please consult http://www.elsevier.com/artworkinstructions.

Any queries or remarks that have arisen during the processing of your manuscript are listed below and highlighted by flags in the proof. Click on the 'Q' link to go to the location in the proof.

Location in article	Query / Remark: click on the Q link to go Please insert your reply or correction at the corresponding line in the proof
Q1	Please check telephone/fax number of the corresponding author, and correct if necessary.
Q2	"Research Highlights should consist of only 85 characters per bullet point, including spaces. However, the research highlights provided for this item exceed the maximum requirement; thus, they were not captured. Kindly provide the necessary corrections. For more information, please see Guide for Authors."
Q3	As per journal style, the rest of the journal titles in the references were abbreviated for consistency. Please check if the abbreviations used are acceptable.
Q4	As per journal style, the rest of the journal titles in the references were abbreviated for consistency. Please check if the abbreviations used are acceptable.
Q5	As per journal style, the rest of the journal titles in the references were abbreviated for consistency. Please check if the abbreviations used are acceptable.
Q6	Please update the status of this reference by providing volume number, issue and pagination details or DOI.
Q7	As per journal style, the rest of the journal titles in the references were abbreviated for consistency. Please check if the abbreviations used are acceptable.
Q8	As per journal style, the rest of the journal titles in the references were abbreviated for consistency. Please check if the abbreviations used are acceptable.
Q9	As per journal style, the rest of the journal titles in the references were abbreviated for consistency. Please check if the abbreviations used are acceptable.
Q10	As per journal style, the rest of the journal titles in the references were abbreviated for consistency. Please check if the abbreviations used are acceptable.
Q11	As per journal style, the rest of the journal titles in the references were abbreviated for consistency. Please check if the abbreviations used are acceptable.
Q12	As per journal style, the rest of the journal titles in the references were abbreviated for consistency. Please check if the abbreviations used are acceptable.

Q13	As per journal style, the rest of the journal titles in the references were abbreviated for consistency. Please check if the abbreviations used are acceptable.
Q14	Figures 2, 3, 5 and 6 contain pixelated text. Please check and provide replacement if deemed necessary.

Thank you for your assistance.

Powder Technology xxx (2010) xxx

Contents lists available at ScienceDirect

Powder Technology

journal homepage: www.elsevier.com/locate/powtec

Graphical Abstract

Powder Technology xxx (2010) xxx – xxx

Characterization of mechanically alloyed f.c.c. Ti–Mg-based powders

C. Machio [a,*], D. Nyabadza [b], V. Sibanda [b], H.K. Chikwanda [a]

[a] Council for Scientific and Industrial Research, P.O. Box 395 PRETORIA 0001, Republic of South Africa
[b] School of Chemical and Metallurgical Engineering, University of the Witwatersrand, P.O. Private Bag 3, WITS 2050, Republic of South Africa

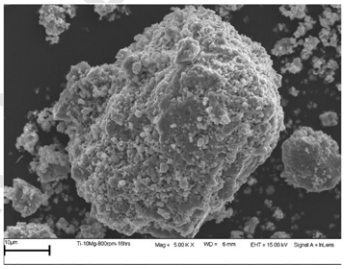

The solubility of Mg in Ti can be increased by high energy ball milling. The milling generates particles of different sizes (shown in this figure) through the interaction of particle fracture, which generates small particles, and agglomeration of the small particles which gives larger particles. Powders of different particle size distributions, and by extension, different thermal and compaction characteristics, can be produced.

0032-5910/$ – see front matter © 2010 Elsevier B.V. All rights reserved.
doi:10.1016/j.powtec.2010.11.023

Powder Technology xxx (2010) xxx–xxx

Contents lists available at ScienceDirect

Powder Technology

journal homepage: www.elsevier.com/locate/powtec

Characterization of mechanically alloyed f.c.c. Ti–Mg-based powders

C. Machio [a,*], D. Nyabadza [b], V. Sibanda [b], H.K. Chikwanda [a]

[a] Council for Scientific and Industrial Research, P.O. Box 395 PRETORIA 0001, Republic of South Africa
[b] School of Chemical and Metallurgical Engineering, University of the Witwatersrand, P.O. Private Bag 3, WITS 2050, Republic of South Africa

ARTICLE INFO

Article history:
Received 18 May 2010
Received in revised form 30 September 2010
Accepted 20 November 2010
Available online xxxx

Keywords:
Ti–Mg alloys
Mechanical alloying
Green density

ABSTRACT

Face centred cubic Ti–10 and 20Mg and Ti–6Al–4Mg (wt.%) alloy powders have been produced by high energy ball milling, under argon, of elemental powder mixtures containing a process control agent (PCA). Milling leads to a multi-disperse particle size distribution without affecting the particle morphologies. This affects the thermal stability of the powders and the green densities of compacts. The green densities varied in tandem with the d_{10} sizes of the powders and went through a minimum at 20 h of milling. Milling for 20 h could be detrimental to powder consolidation and further processing.

1. Introduction

Light weight structural materials are increasingly being used for electronics, automotive and aerospace applications. The aerospace industry in particular aspires to decrease the densities of materials used for components because reducing density is the most effective way of lowering the overall weight of a structural component [1]. Even though there is already an extensive use of Ti and its alloys in the aerospace industry because of their low density, there is ongoing research to find even lower density Ti alloys. There is a focus of producing Ti-based alloys in combination with other light metal elements such as magnesium (Mg) and aluminium (Al). Magnesium is particularly attractive since it has a density two-thirds that of Al. Besides structural applications in the transportation industry, Ti–Mg alloys have also been identified as potential materials for hydrogen storage because of their safety, small volume and low weight [2].

The alloying of Ti and Mg has a number of challenges that have already been noted in literature (e.g., [3,4]). These include the fact that the solubility of Mg in Ti is very low. Also, the boiling point of Mg (1380 K) is much lower than the melting point of Ti (1941 K). This temperature difference is important because conventional alloying would involve melting of the elements, and this would lead to substantial losses of Mg. Possible routes to achieve alloying of Ti and Mg are non-equilibrium processes, notably vapor quenching [5] and mechanical alloying [6]. Mechanical alloying is the most popular process and has also been applied to Ti–Mg-based powders, e.g., Ti–Mg–Al [7].

The powders produced by mechanical alloying are consolidated by powder metallurgy (PM) techniques, where they are pressed to form "green compacts," also "green bodies" and then sintered at an appropriate temperature-time combination. The PM process is affected by the characteristics of the powder being processed. On the other hand, the characteristics of the powder are affected by, in this case, the milling parameters.

There is currently an appreciate volume of literature on the mechanical milling of Ti–Mg-based powders, e.g., Refs 4 and 6 where the alloy powders have been produced using attritor and planetary mills and the SPEX milling machines. This powder has been obtained in the hexagonal close packed (h.c.p.) crystal structure form. This work reports on face centred cubic Ti–Mg-based alloy powders that have been produced using a high energy ball mill. Unlike literature, we have linked the effect of one milling parameter, time, to the ease of processing as determined by the densities of the green compacts obtained after cold compaction. This is important because green body densities affect further processing [8].

2. Experimental procedure

2.1. Materials

The nominal composition of powders were Ti–10Mg, and Ti–20Mg and Ti–6Al–4Mg (all compositions in wt.%). The powder mixtures were made from elemental titanium powder (~99.5% purity), elemental magnesium powder (~99.5% purity) and elemental aluminium powder (~99.5% purity), respectively. The material safety data sheets provided the powder particle sizes, determined by sieve analysis, as: 90% of Mg powder particles were less than 71 μm, and 95% of both Al and Ti powder particles were less than 45 μm. To enable comparisons with the mechanically alloyed powders (Section 2.2), the mean sizes of the powders were determined using a laser diffraction technique (Section 2.3) and found to be 25 ± 2 μm, 27 ± 1 μm, and 73 ± 8 μm for Ti, Al and Mg, respectively. These sizes were within the ranges provided by the sieve analysis

* Corresponding author. Tel.: +27 12 841 2870; fax: +27 12 841 3378.
E-mail address: cmachio@csir.co.za (C. Machio).

0032-5910/$ – see front matter © 2010 Elsevier B.V. All rights reserved.
doi:10.1016/j.powtec.2010.11.023

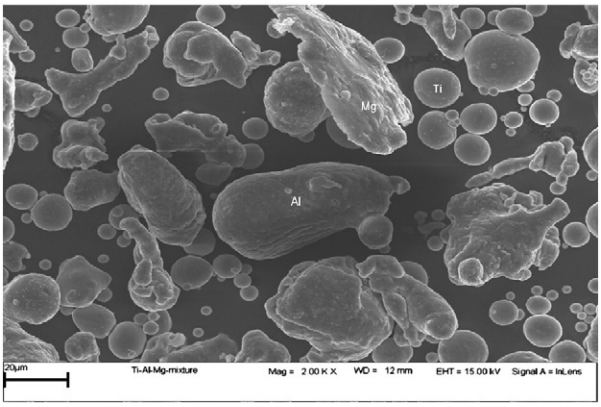

Fig. 1. SEM image of as-blended Ti–Al–Mg powder mixture. Particles identified using EDS in SEM. Titanium powder particles are spherical, aluminium particles are nodular and magnesium powder particles are platy.

performed by the powder suppliers. The morphologies of the particles of the Ti, Mg, and Al powders, obtained using scanning electron microscopy (Section 2.3), were spherical, platy and nodular, respectively (Fig. 1).

2.2. Mechanical alloying

Carefully weighed elemental metal powder and process control agent (PCA) mixtures were milled at room temperature in a Simoloyer CM01-2l high energy ball mill using a rotation speed of 800 rpm, a ball-to-powder (mass) ratio (BPR) of 20:1 and uninterrupted milling periods of 16, 20, 24 and 32 h. These periods were selected to allow complete alloying and homogenization. The grinding media were 5-mm diameter DIN 100Cr6 chrome steel balls. Each milling run used 100 g of powder mixture to which 8 wt.% stearic acid, the PCA, was added. The PCA reduces cold welding of powder particles and their adhesion to the milling chamber walls and grinding media (balls). To minimise powder oxidation, milling was carried out under an argon atmosphere.

2.3. Powder characterisation

Milled powders were characterized for phases using a Phillips PW 1710 X-ray Diffractometer equipped with a Phillips Analytical X'pert Highscore software for identifying phases. A monochromatic *Cu-Kα* radiation was used at 40 kV and 20 mA. The crystallite sizes of the milled powders were approximated using the Scherrer equation [9] and parameters of the main peak on the respective XRD patterns, in line with literature on milling of powders [10,11]. The crystallite sizes were determined only for comparison purposes because the Scherrer equation does not consider the effect of strain and the sizes obtained have a large margin of error [11]. However, the trend of variation of the sizes is similar to that obtained by other models like the Williamson–Hall method [12]. Prior to the acquisition of patterns, the XRD was calibrated using a silicon single crystal. Powder particle morphologies were determined using a JEOL JSM-6510 Scanning Electron Microscope (SEM). The Mg content in the powders was approximated from a semi-quantitative SEM energy dispersive spectroscopy (SEM-EDS) analysis using 10 different fields of view. The size and size distributions of the particles were determined using a Microtrac® Bluewave particle size analyser. Two samples were used for each powder to determine the reproducibility of the particle size distributions.

The thermal behavior of the powders was determined in the range room temperature to 660 °C in an argon atmosphere using a simultaneous thermal analyzer (Netzsch STA 449 F3 *Jupiter*). The heating rate was 10 °C/min and the samples were furnace cooled to room temperature after the maximum temperature was attained.

2.4. Powder compaction

The powders were compacted at room temperature using a hand operated uni-axial press set to either 27 or 33 MPa. These translated to pressures of 270 and 330 MPa, respectively. Four compacts were pressed from each powder. The densities of the compacts were determined using their weights and dimensions, and presented as averages.

3. Results and discussion

3.1. Phases in alloy powders

The XRD patterns of milled Ti–10Mg and Ti–20Mg powders are given in Figs. 2 and 3, respectively. All the patterns of the Ti–10Mg powders had peaks of the same phase. The Ti and Mg peaks observed in the unmilled Ti–10Mg powder mixture disappeared after 16 h of milling

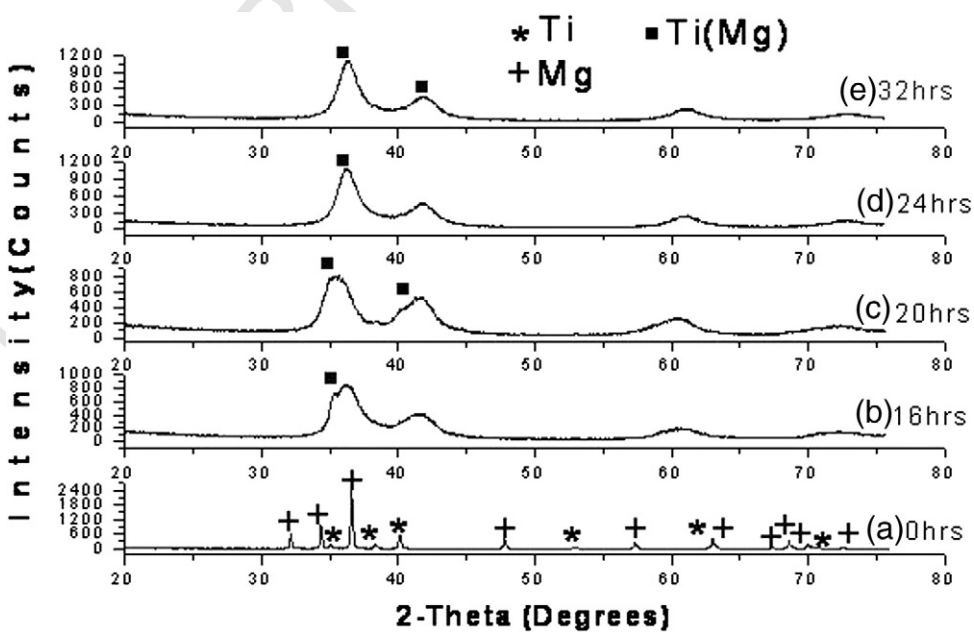

Q14 **Fig. 2.** XRD patterns of Ti–10Mg powders milled for (a) 0 h, (b) 16 h, (c) 20 h, (d) 24 h, and (e) 32 h. The unlabelled peaks on the XRD patterns of the milled powders belong to TiMg solid solution.

Please cite this article as: C. Machio, et al., Characterization of mechanically alloyed f.c.c. Ti–Mg-based powders, Powder Technol. (2010), doi:10.1016/j.powtec.2010.11.023

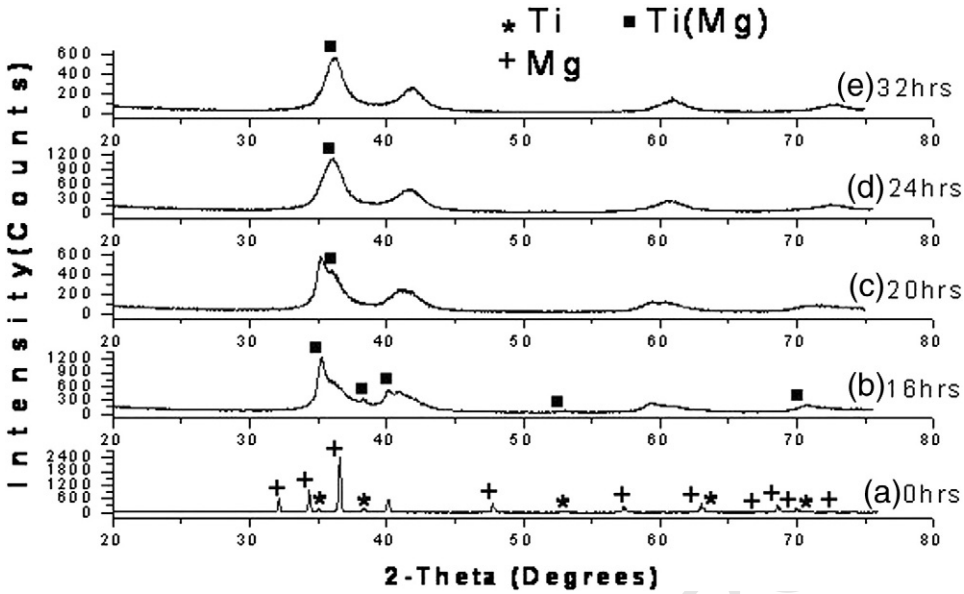

Fig. 3. XRD patterns of Ti–20Mg powders milled for (a) 0 h, (b) 16 h, (c) 20 h, (d) 24 h, and (e) 32 h.

indicating the formation of a TiMg solid solution having peaks at ≈36° (2θ) (major peak) and ≈41.9° (2θ) (minor peak). On the other hand, the XRD pattern for Ti–20Mg powder milled for 16 h (Fig. 3) had poorly formed TiMg peaks, unlike the case for Ti–10Mg. This indicates that alloying was delayed in the Ti–20Mg powders. This happened because a higher amount of energy is required to force increasingly higher amounts of Mg into the Ti crystal structure. When the energy imparted to the powder mixtures is less as occurs when the milling time and/or speed are low, only a small amount of Mg enters the Ti lattice [13]. Further milling of the Ti–20Mg powders led to the formation of peaks similar to those of Ti–10Mg, indicating the complete formation of a TiMg solid solution.

Reitveld analysis showed that the milled Ti–Mg powders all had a face centred cubic (f.c.c.) crystal structure (Fig. 4) and that the patterns could be approximated by f.c.c. Ti–(≈7 wt.%)Mg alloy. The observation of the f.c.c. Ti–Mg solid solution here is unlike literature where the Ti–Mg alloy powder has been found to have an h.c.p. crystal structure [6,13,14]. These differences can be attributed to the fact that earlier researchers used the SPEX 8000 milling machine, while the present work has been done using a Simoloyer CM01-2l high energy ball milling machine. The Simoloyer CM01-2l is more energetic than the SPEX 8000 [15].

The XRD patterns of milled Ti–6Al–4Mg are shown in Fig. 5. All the elemental peaks had disappeared after 16 h of milling and on subsequent milling, suggesting that a solid solution, Ti–(Al,Mg), had formed. The position of peaks of the alloy powders were similar to the position of peaks for milled Ti–10Mg and Ti–20Mg (Figs. 2 and 3), implying that the crystal structure of the Ti–(Al,Mg) solid solution is also f.c.c. The formation of an f.c.c. crystal structure is unlike literature where milled Ti–Al–Mg powder have been reported to have an h.c.p. crystal structure [7]. As was the case for Ti–Mg above, the Ti–Al–Mg powder referred to had been milled in a planetary ball mill, which is less energetic than the SPEX 8000 mill already mentioned above [16] and is therefore much less energetic compared to the Simoloyer CM01 used in the current study [15].

The formation of f.c.c. solid solutions in both the TiMg and Ti–6Al–4Mg powders observed here is similar to milled Ti–Al powders [17]. This occurrence is attributed to the polymorphic h.c.p. to f.c.c. transformation that occurs for high energy milled h.c.p. Ti [10,17] powder. The h.c.p. → f.c.

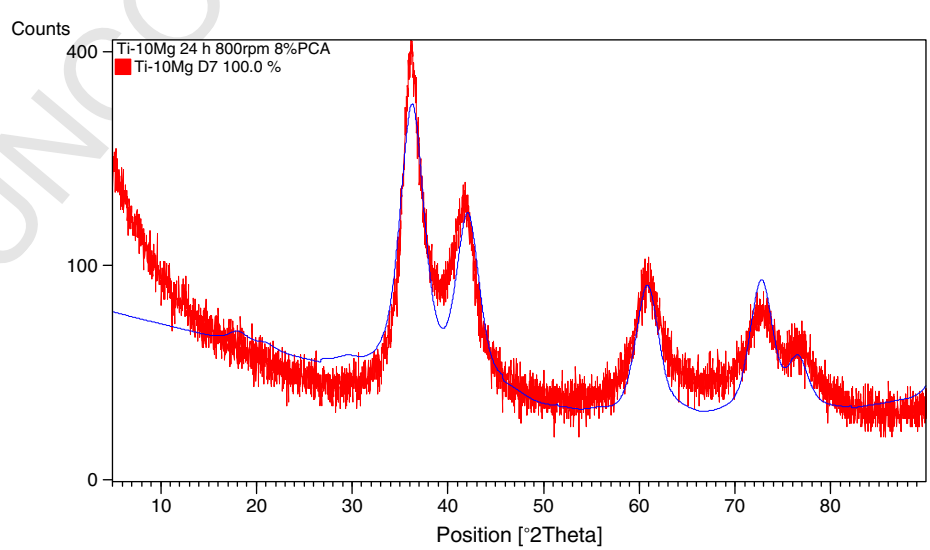

Fig. 4. Experimental and Reitveld-fitted XRD patterns of a Ti–Mg powder milled for 24 h. Similar fitted patterns were obtained for the powders milled for 16, 20 and 32 h.

Please cite this article as: C. Machio, et al., Characterization of mechanically alloyed f.c.c. Ti–Mg-based powders, Powder Technol. (2010), doi:10.1016/j.powtec.2010.11.023

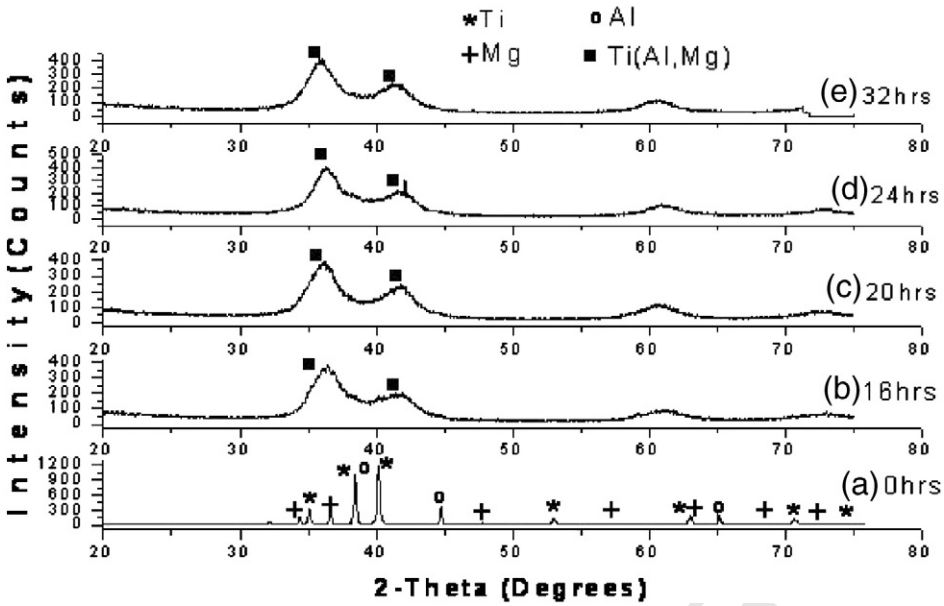

Fig. 5. XRD patterns of Ti–6Al–4Mg powders milled for (a) 0 h, (b) 16 h, (c) 20 h, (d) 24 h, and (e) 32 h. Peaks on the XRD patterns of milled powders are for Ti(Al,Mg).

c. Ti transformation is accompanied by an increase in volume of the crystal unit cell [10], and it this increase that can account for the observed high solubility of Mg in Ti. It is difficult to have higher amounts of Mg in Ti in milling events where the Ti remains h.c.p. after milling [13].

The XRD peaks of the f.c.c. phase formed after milling were broadened and similar to other milled powders [7,11,18]. The peak broadening is associated with a decrease in the size of the crystallites interacting with X-rays to the nanometer range and plastic strain in the powder particles. Table 1 gives crystallite sizes for the powders in this study. The sizes, which are comparable to those found in literature [6,19], decreased with increasing milling time, a phenomenon that is also in line with literature of other milled powders [18]. However, unlike an earlier study where the crystallite size decreased with Mg content, in the current study, the crystallite size is independent of the magnesium content [6]. In general, the crystallite size is a function of the amount of plastic deformation, which determines the amount of crystal defects that form in the material being milled and the possible recovery process, and is dependent only on the melting point of the alloy [20].

3.2. Powder particle morphologies and mg content

All the milled powders had a collection of both small and large particles. The particle shapes was a mixture of globular, granular and irregularly shapes, similar to literature [6]. Fig. 6 (for Ti–10 wt.% Mg) shows representative morphologies. The particles also appeared rougher and this was found to have been due to the collection of smaller particles on the surfaces of other larger particles (Fig. 7).

Table 2 gives the Mg content of the milled powders. While the overall composition of each powder was close to the nominal composition, the standard deviations showed the compositions of the powders varied from point to point. This chemical heterogeneity is common for milled powders [21]. It probably occurs because of the lack of extensive diffusion that is required to allow a redistribution of atoms to eliminate concentration gradients. The solute atoms ordinarily segregate at the grain boundaries [22].

Table 1
Crystallite sizes of milled powders.

Milling time (h)	Crystallite size[1] (nm)		
	Ti–10Mg	Ti–20Mg	Ti–6Al–4Mg
16	22.0	24.6	-
20	18.0	13.9	11
24	9.2	10.1	10
32	9.2	8.3	-

[1] Only the major peak of each powder was used to determine the grain sizes.

3.3. Particle size analysis

Figs. 8–10 show the characteristic normal size distribution curves for the milled powders. Size in this case refers to the diameters of the powder particles. Compared to before milling, the curves for the milled powders were shifted to the left, i.e., to smaller values. The powder blends before milling were mono-disperse while the milled powders were multi-disperse, with the degree of multi-dispersion depending on the milling time. The Ti–10 wt.% and Ti–6Al–4Mg (wt.%) milled for 20 h had a tri-modal particle size distribution, implying the presence of very small particles (fines) while milling for the other durations led to powders with a bi-modal particle size distribution. On the other hand, the milled Ti–20Mg (wt.%) powders were only bi-modal and without any fines.

The d_{10}, d_{50} and d_{90} particle sizes are provided in Tables 3–5. The initial milling of 16 h led to a substantial decrease of powder particle size. However, the rate of decrease slowed down on continued milling and particle size values went through a minimum before gradually increasing and becoming independent of the milling time on continued milling, as shown in Fig. 11 for the mean sizes (d_{50}).

The evolution of particle size during milling observed here, as in other milling work, is a function of two competing processes: particle fragmentation and agglomeration through cold welding [23]. An initial steep decrease of particle size occurs due to particle fragmentation. In the current study, the process of fragmentation continued to about 20 h of milling (Fig. 11). At the same time, agglomeration by cold welding was starting to occur. While fragmentation dominated agglomeration during milling up to 20 h, longer milling resulted in agglomeration dominating fragmentation. This led to a slight increase of particle size (Fig. 11). It would have been expected that the agglomeration produced larger particles, but this is stopped by the development of a steady state between fragmentation and agglomeration. The steady state situation leads to the particle size becoming independent of the milling time (Fig. 11), and is line with literature [11]. The mean particle size (d_{50}) of

Please cite this article as: C. Machio, et al., Characterization of mechanically alloyed f.c.c. Ti–Mg-based powders, Powder Technol. (2010), doi:10.1016/j.powtec.2010.11.023

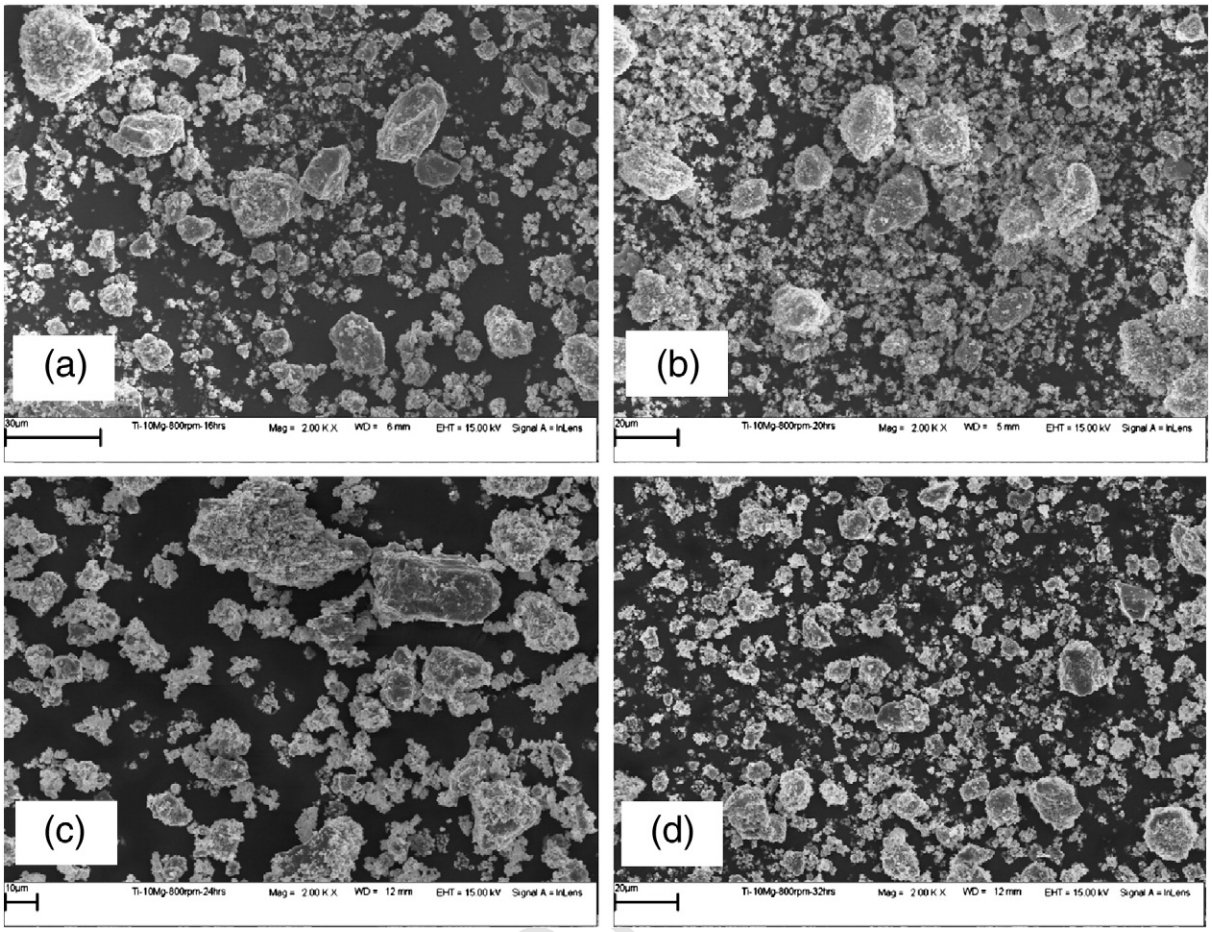

Fig. 6. SEM micrographs of Ti–10Mg powders milled for (a) 16 h, (b) 20 h, (c) 24 h, and (d) 32 h.

the powders appeared to converge to the same value after 32 h of milling, implying that the particle size evolution on continued milling was determined by the Ti, which was present in larger quantities.

The slight agglomeration observed on milling beyond 20 h occurred probably because the PCA became less effective on longer milling due to decomposition [24]. The fact that the fracturing process appears to have peaked at 20 h can explain the occurrence of the tri-modal particle size distribution observed in Figs. 8–10. The formation of the finer particles in Ti–20Mg appears to have been mitigated by the presence of a larger volume fraction of the coarser Mg powder.

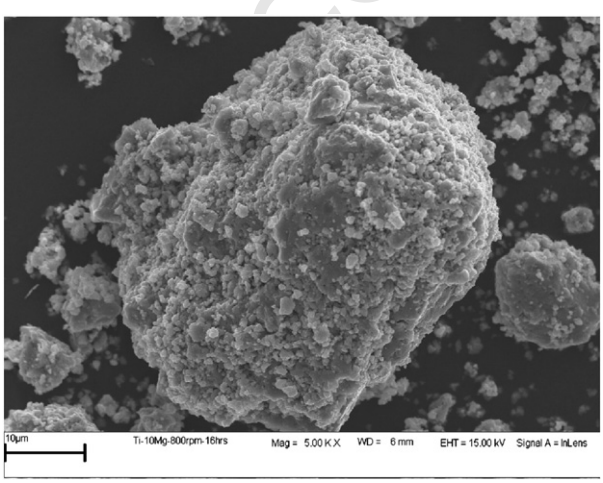

Fig. 7. Roughened appearance of large particles was caused by a collection of smaller particles on the surfaces of other particles.

3.4. Thermal behavior

Fig. 12 shows the characteristic thermal behavior of both the Ti–Mg and Ti–6Al–4Mg milled powders. All the graphs have a broad endothermic peak centred at around 100 °C that was probably caused by the evaporation of the PCA, which had been intentionally added to aid in the milling process (Section 2.2). The thermal behaviors of the of the Ti–10Mg powders milled for 16, 24 and 32 h were similar, with a characteristic appearance as shown in Fig. 12a for powder milled for 16 h. A broad exothermic peak between 100 °C and 430 °C preceded a sharp exothermic peak at around 480 °C and a sharp endothermic peak at about 648 °C. In contrast, the powders milled for 20 h were characterized by two broad exothermic peaks between 100 °C and 430 °C, centred at 291 °C and 405 °C, respectively. These were followed by smaller exothermic peaks at 497 °C and 542 °C. There were also endothermic peaks centred at 359 °C and 517 °C. In

Table 2
Mg and Al contents of milled powders as determined by EDS.

Milling time (h)	Mg content (wt.%)			Al content (wt.%)
	Ti–10Mg	Ti–20Mg	Ti–6Al–4Mg	Ti–6Al–4Mg
16	8.9 ± 0.6	16.6 ± 0.8	4.0 ± 0.3	6.5 ± 0.4
20	8.5 ± 0.6	16.8 ± 1.0	4.1 ± 0.6	6.5 ± 0.9
24	9.0 ± 0.5	16.4 ± 1.2	3.7 ± 0.3	5.9 ± 0.5
32	9.0 ± 1.0	17.9 ± 0.8	3.8 ± 0.3	5.6 ± 0.3

Please cite this article as: C. Machio, et al., Characterization of mechanically alloyed f.c.c. Ti–Mg-based powders, Powder Technol. (2010), doi:10.1016/j.powtec.2010.11.023

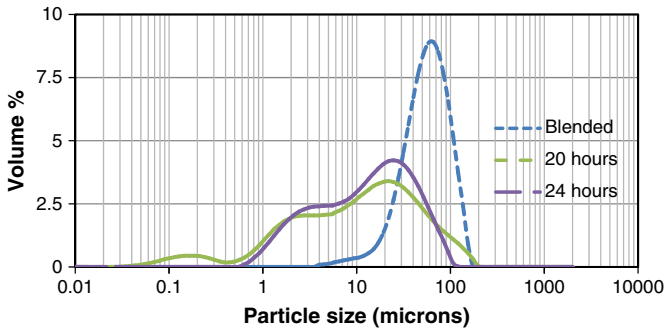

Fig. 8. Particle size distribution curves for milled Ti–10Mg powders.

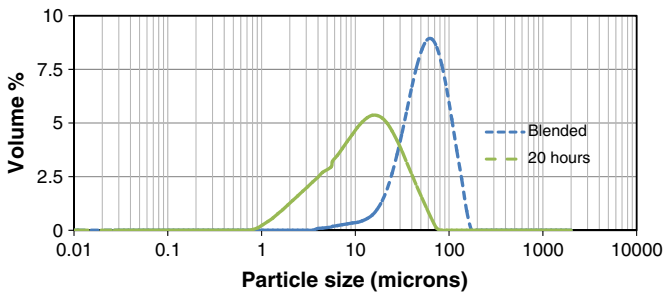

Fig. 9. Particle size distribution curves for milled Ti–20Mg powders.

comparison to the Ti–10Mg powders, the Ti–20Mg powders had very similar curves regardless of the milling time (of 16, 20, 24, and 32 h). These were characterized by a broad exothermic peak between 100 °C and 500 °C, followed by an exothermic peak at about 527 °C as shown for powders milled for 16 and 20 h (Fig. 12b).

The thermal behaviors of the Ti–6Al–4Mg powders were similar to those of the Ti–10Mg powders. The powders milled for 16, 24, and 32 h had one broad exothermic peak between 100 °C and 550 °C, centred at approximately 330 °C, followed by an endothermic peak at 548 °C and by another exothermic peak at 592 °C. On the other hand, the powders milled for 20 h had two exothermic peaks between 100 °C and 550 °C, centred at 290 °C and 410 °C respectively, followed by an endothermic peak at 528 °C (Fig. 12c).

The very broad exothermic peaks on the thermograms of all the powders at lower temperatures can be associated with the occurrence of recovery processes, which help release the strain energy stored in the powders due to the milling process [25]. On the other hand, the very sharp exothermic peaks obtained for both the Ti–10Mg and Ti–20Mg powders (milled for 16, 24, and 32 h) (Fig. 12a and b) could have been caused by the decomposition of the supersaturated TiMg solid solutions. Similar sharp exothermic peaks are not obtained for the Ti–6Al–4Mg powders because the level of saturation is less since Ti dissolves some Al and the Al also dissolves some Mg under equilibrium conditions. It could also be argued that the sharp exothermic peaks on the curves for the Ti–Mg

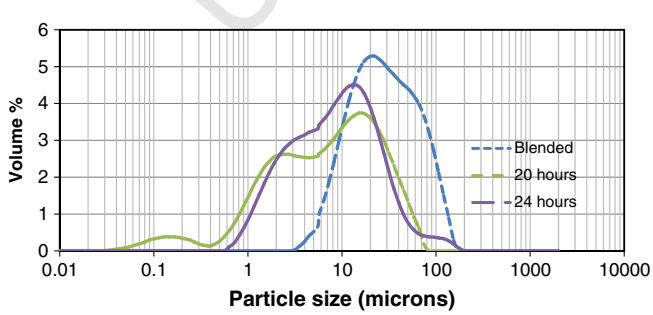

Fig. 10. Particle size distribution curves for milled Ti–6Al–4Mg powders.

Table 3
Particle size distribution of Ti–10Mg powders.

Milling time	d_{10} (μm)	d_{50} (μm)	d_{90} (μm)
0 h	24.1 ± 0.2	53.4 ± 0.5	104.3 ± 3.5
16 h	1.7 ± 0.1	9.5 ± 0.1	38.2 ± 6.8
20 h	1.1 ± 0	10.6 ± 0.7	50.8 ± 8.9
24 h	1.6 ± 0.3	11.3 ± 0.4	43.8 ± 3.1
32 h	1.5 ± 0.3	12.6 ± 0.2	52.2 ± 3.5

Table 4
Particle size distribution of Ti–20Mg powders.

Milling time	d_{10} (μm)	d_{50} (μm)	d_{90} (μm)
0 h	25.2 ± 0.3	46.2 ± 0.7	106.9 ± 1.5
16 h	3.3 ± 0.4	13.8 ± 0.4	38.3 ± 1.1
20 h	2.9 ± 0	11.7 ± 0.1	32.2 ± 0.4
24 h	3.1 ± 0.2	13.8 ± 1.5	45.1 ± 12.7

Table 5
Particle size distribution of Ti–6Al–4Mg powders.

Milling time	d_{10} (μm)	d_{50} (μm)	d_{90} (μm)
0 h	8.9 ± 0.2	25.2 ± 0.6	76.0 ± 1.0
16 h	1.8 ± 0.2	10.7 ± 0.5	33.5 ± 1.9
20 h	0.8 ± 0.2	6.8 ± 0.4	28.7 ± 1.7
24 h	1.6 ± 0.3	8.5 ± 0.4	28.5 ± 0.3
32 h	1.3 ± 0.3	11.5 ± 1.7	45.0 ± 7.0

powders were caused by a reduction of the grain boundary area due to the growth or coarsening of the nanosize grains. However, this does not appear to be the case since the curves of the Ti–6Al–4Mg powders did not have similar sharp exothermic peaks yet they also had nanosize grains (Table 1). Also, it has been shown that grain growth/coarsening is not associated with a large enthalpy change [26]. On the other hand, similar exothermic peaks have been associated with a phase change [27] for milled Fe–Cu powders, which, like the Ti–Mg powders in this study, are immiscible under equilibrium conditions. It is therefore possible that a similar phenomenon is occurring for the Ti–Mg powders in this study, and will be investigated. The smaller exothermic events for Ti–10Mg and Ti–6Al–4Mg powders milled for 20 h could be decomposition events brought about by varying powder particle size.

The endothermic peaks at approximately 359 °C and 517 °C on the curves of the Ti–10Mg powder milled for 20 h were probably caused by the melting of the fines that were generated during milling (Figs. 8 and 9). The same can be said of the endothermic peak at approximately 370 °C on the curve for the Ti–6Al–4Mg powder milled for 20 h. The endothermic peak at about 550 °C for the Ti–6Al–4Mg powders milled for 16, 24 and

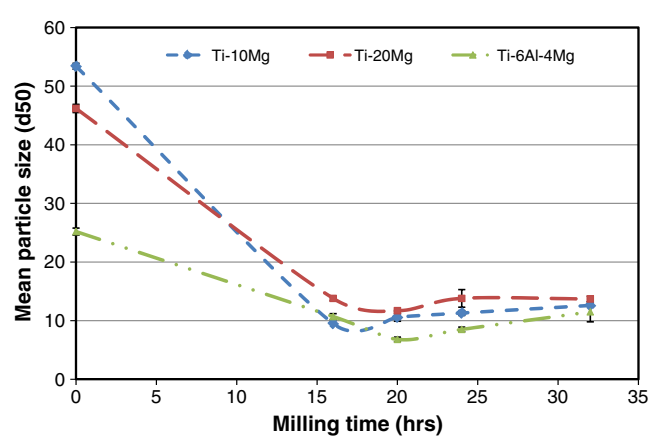

Fig. 11. Variation of mean particle size (d_{50}) with milling time.

Please cite this article as: C. Machio, et al., Characterization of mechanically alloyed f.c.c. Ti–Mg-based powders, Powder Technol. (2010), doi:10.1016/j.powtec.2010.11.023

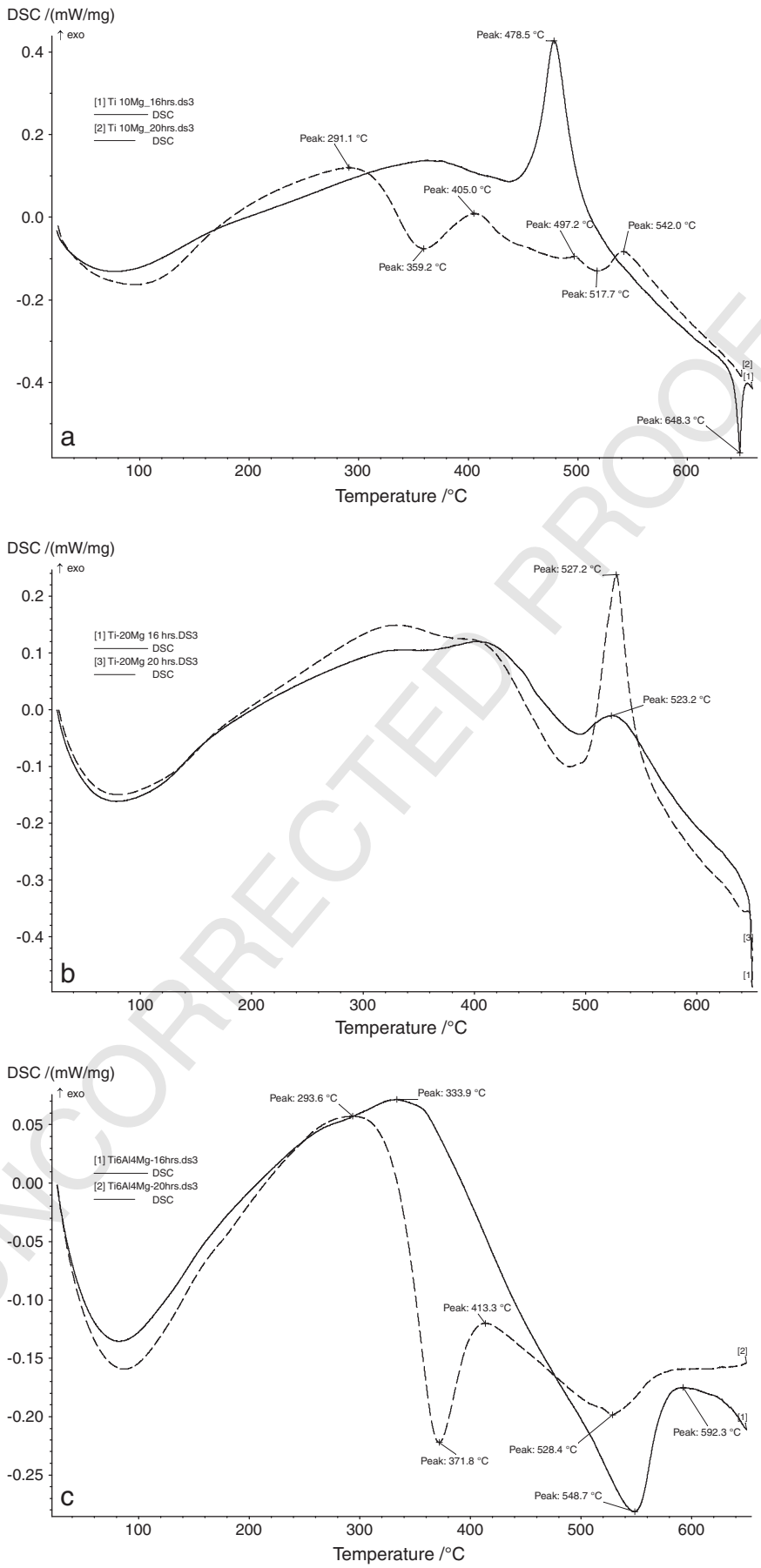

Fig. 12. Thermal behavior of milled powders (a) Ti–10Mg, (b) Ti–20Mg, and (c) Ti–6Al–4Mg.

Please cite this article as: C. Machio, et al., Characterization of mechanically alloyed f.c.c. Ti–Mg-based powders, Powder Technol. (2010), doi:10.1016/j.powtec.2010.11.023

32 h and a similar peak at about 530 °C on the curve of the powder milled for 20 h were probably caused by the melting of Al whose melting point is decreased by milling [18], while the sharp endothermic peak at about 648 °C on the curves for Ti–10Mg (wt.%) powders is associated with the melting of Mg.

3.5. Green density and compaction effects

The green densities after compaction went through a minimum at 20 h (Fig. 13) and mirrors the variation of the mean particle size of the 10th percentile (d_{10}) (Tables 3–5) which for all the powders went through a minimum at 20 h. This indicates that the green densities were a function of the amount of the fine particles in each milled powder, and not necessarily the mean particle size (d_{50}). As already noted, the d_{50} values of all the powders converged to a similar value with continued milling up to 32 h (Fig. 11). In general, powders with fine particles are associated with lower green densities [28].

The variation of green density with milling time (Fig. 13) is similar to the variation of tap density with milling time. The suggestion in literature is that this variation is caused by the evolution of morphology from spherical through lamellar back to spherical [29]. This sequence of evolution was not observed in the current study, where the powder particle morphologies of the different powders were similar (Figs. 6 and 7).

The green density is an important parameter for materials processed by the powder metallurgical route because it affects the properties of the sintered components. Ideally, the green density needs to be as high as possible [30]. It is possible that the low densities obtained for the powders milled for 20 h can be detrimental to further processing steps.

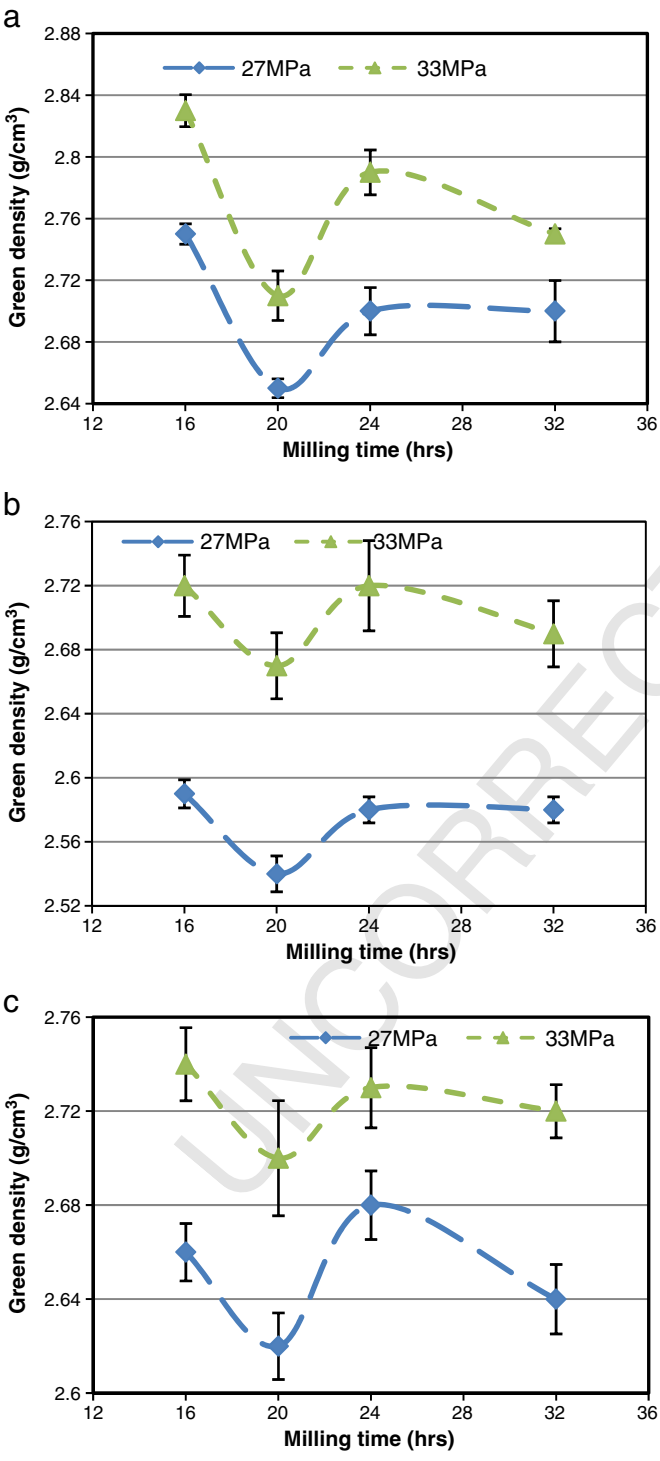

Fig. 13. Variation of green density with milling time and compaction pressure: (a) Ti–10Mg, (b) Ti–20Mg, and (c) Ti–6Al–4Mg.

4. Conclusions

This work has shown that high energy milling of Ti–10Mg, Ti–20Mg, and Ti–6Al–4Mg powder mixtures lead to the formation of f.c.c. Ti-based alloy powders whose crystallite size decreases with milling time. The particle size distribution is dependent on the milling time and Mg content. Milling for 20 h produces tri-modal particle size distribution with very fine particles compared to bi-modal distributions for the other milling durations and for higher Mg contents. The fine particles formed after milling for 20 h lead to the appearance of more thermally induced events leading to more exothermic peaks during heating. The thermal behavior of the powders is however more complicated and further experimental work is continuing to provide a better understanding of the behavior. The milling time needs to be optimized for any alloy system since it affects green densities and further processing of the milled powder.

Acknowledgements

The Department of Science and Technology (DST) and the Council for Industrial and Scientific Research (CSIR), South Africa are acknowledged for the overall funding of the work. The DST's Center of Excellence in Strong Materials (CoE-SM), University of the Witwatersrand, is acknowledged for funding Mr D. Nyabadza's MSc studies. Mr. Tafadza Mushove is acknowledged for assisting with the some of the powder characterization work.

References

[1] J.C. Ekvall, J.E. Rhodes, G.G. Wald, Methodol. evaluating weight savings basic material properties (1982) 328–341.
[2] Y. Zhang, Y. Tsushio, H. Enoki, E. Akiba, J. Alloy. Comp. 393 (1-2) (2005) 185–193.
[3] R. Sundaresan, F.H. Froes, Key Eng. Mater. 29-31 (1989) 199–206.
[4] C. Suryanarayana, F.H. Froes, J. Mater. Res. 5 (9) (1990) 1880–1886.
[5] C.M. Ward-Close, G. Lu, P.G. Partridge, Mater. Sci. Eng. A 189 (1994) 247–255.
[6] F. Sun, F.H. (Sam) Froes, J. Alloy. Comp. 340 (1-2) (2002) 220–225.
[7] M. Caetano, B. Trindade, J. Mater. Sci. 42 (18) (2007) 7684–7689.
[8] J.L. Woolfrey, J. Am. Ceram. Soc. 55 (8) (1972) 383–389.
[9] A.L. Patterson, Phys. Rev. 56 (10) (1939) 972–977.
[10] I. Manna, P.P. Chattopadhyay, P. Nandi, F. Banhart, H.-J. Fecht, J. Appl. Phys. 93 (3) (2003) 1520–1524.
[11] V.V. Dabhade, T.R. Rama Mohan, P. Ramakrishnan, Powder Technol. 171 (3) (2007) 177–183.
[12] V.d.P. Martínez, C. Aguilar, J. Marín, S. Ordoñez, F. Castro, Mater. Lett. 61 (4-5) (2007) 929–933.
[13] E. Zhou, C. Suryanarayana, F.H. (Sam) Froes, Mater. Lett. 23 (1–3) (1995) 27–31.
[14] D.M.J. Wilkes, P.S. Goodwin, C.M. Ward-Close, K. Bagnall, J. Steeds, Mater. Lett. 27 (1-2) (1996) 47–52.
[15] Zoz, H., Vernet, I., Jaramillo-Vigueras, D., PM2TEC'2003; 2003; MPIF; 2003.
[16] C. Suryanarayana, Prog. Mater. Sci. 46 (1–2) (2001) 1–184.
[17] C. Suryanarayana, G. Chen, F.H. (Sam) Froes, Scr. Metall. Mater. 26 (11) (1992) 1727–1732.

Please cite this article as: C. Machio, et al., Characterization of mechanically alloyed f.c.c. Ti–Mg-based powders, Powder Technol. (2010), doi:10.1016/j.powtec.2010.11.023

[18] M. Mhadhbi, M. Khitouni, M. Azabou, A. Kolsi, Mater. Charact. 59 (7) (2008) 944–950.
[19] B. Trindade, M. Caetano, N. Duarte, Mater. Sci. Forum 514-516 (2006) 609–613.
[20] C.C. Koch, Nanostruct. Mater. 9 (1–8) (1997) 13–22.
[21] Y. Jiraskova, K. Zabransky, I. Turek, J. Bursik, D. Jancik, J. Alloy. Comp. 477 (1-2) (2009) 55–61.
[22] C.C. Koch, Nanostruct. Mater. 2 (2) (1993) 109–129.
[23] J.S. Benjamin, T.E. Volin, Metall. Trans. 5 (8) (1974) 1929–1934.
[24] S. Kleiner, F. Bertocco, F.A. Khalid, O. Beffort, Mater. Chem. Phys. 89 (2-3) (2005) 362–366.
[25] G. Liang, R.S. Schultz, J. Mater. Sci. 38 (6) (2003) 1179–1184.
[26] F. Zhou, X.Z. Liao, Y.T. Zhu, S. Dallek, E.J. Lavernia, Acta Mater. 51 (10) (2003) 2777–2791.
[27] J. Eckert, J.C. Holzer, W.L. Johnson, J. Appl. Phys. 73 (1) (1993) 131.
[28] E.J. Gonzalez, G.J. Piermarini, in: Hari Singh Nalwa (Ed.), Handbook of nanostructured materials and nanotechnology, Academic Press, Burlington, 2000.
[29] J.B. Fogagnolo, E.M. Ruiz-Navas, M.H. Robert, J.M. Torralba, Mater. Sci. Eng. A 355 (1–2) (2003) 50–55.
[30] S. Giménez, A. Vagnon, D. Bouvard, O. Van der Biest, Mater. Sci. Eng. A 430 (1-2) (2006) 277–284.

Please cite this article as: C. Machio, et al., Characterization of mechanically alloyed f.c.c. Ti–Mg-based powders, Powder Technol. (2010), doi:10.1016/j.powtec.2010.11.023